(Preprint) AAS 23-218

CONTINUOUS CENTER-OF-MASS ESTIMATION FOR A GIMBALED ION-THRUSTER EQUIPPED SPACECRAFT

R. Calaon[*], C. Allard[†] and H. Schaub[‡]

Knowledge of the location of the center of mass of a spacecraft is an essential piece of information at flight software level, because it influences the definition of the requirements from the attitude control subsystem. While the location of the center of mass is typically known at the beginning of a mission, it can change over time. With electric propulsion, it is necessary to know precisely along which direction to fire the thruster, in order to avoid the accumulation of momentum that would ultimately lead to reaction wheel saturation. This study involves an ion thruster that is fired along an inertially-fixed direction to perform a long-term maneuver correction, while the orientation of the spacecraft is stabilized with reaction wheels. This paper investigates using the steady-state integral feedback term of the attitude control law to inform a sequential least squares estimator about the location of the center of mass, which is estimated continuously. Results illustrate that with even small degree-level thruster platform orientation changes the three-dimensional center of mass location can be estimated.

INTRODUCTION

Over the course of a space mission, the location of the center of mass (CM) changes due to various reasons. The dominant contributor is typically mass depletion, when propellant is expelled to provide thrust. Additionally, in complex spacecraft designs that involve moving appendages, the center of mass varies as such appendages are moved with respect to the spacecraft hub, thus adding uncertainty to the accuracy on the CM location. The location of the CM of the system is a vital piece of information that affects the computation of the requested forces in thruster-based control. An incorrect CM estimate results in the wrong force request delivered to the thruster(s), and consequently the inability to bring the spacecraft to the desired state.

Modern spacecraft designs often involve the presence of electric thrusters given their high specific impulse, and consequent lower propellant mass requirement.[1] The tradeoff consists in the fact that these thrusters typically need to operate for extended periods of time. In such circumstances, a good CM location estimate becomes relevant because a misalignment between the CM and the thrust vector produces undesired torques on the system, which have to be compensated by the reaction wheels (RWs). Some of the more recent mission designs have explored the idea of mounting the electric thruster on a dual-gimbal mechanism that allows the direction of the thrust vector to

[*]Ph.D. Candidate, Ann and H.J. Smead Department of Aerospace Engineering Sciences, University of Colorado, Boulder, 3775 Discovery Drive, Boulder, CO, 80303. AIAA Student Member.

[†]Guidance, Navigation and Control Engineer, Laboratory for Atmospheric and Space Physics, 1234 Innovation Dr, Boulder, CO 80303.

[‡]Professor and Department Chair, Schaden Leadership Chair, Ann and H.J. Smead Department of Aerospace Engineering Sciences, University of Colorado, Boulder, 431 UCB, Colorado Center for Astrodynamics Research, Boulder, CO, 80309. AAS Fellow, AIAA Fellow.

be controlled with respect to the spacecraft hub. In principle, this was motivated by the need to adjust the thrust direction based on the system's center of mass as it changes over time.[2,3] More recent studies[4] and mission concepts[5] are also studying the possibility of intentionally offsetting the thruster with respect to the CM in order to perform continuous momentum dumping. This would prove beneficial in the long term, as it would limit the impact of external forces and torques on actuator saturation.

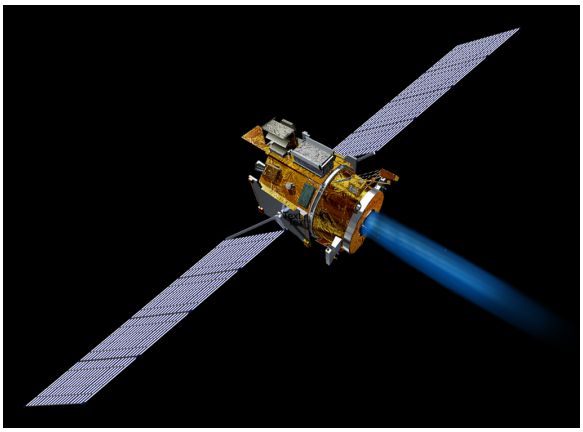

Figure 1: Artistic rendering of the Deep Space 1 spacecraft, featuring an ion engine

Whether the goal is to perform continuous momentum dumping, or to produce zero net torque on the system, accurate knowledge of the location of the center of mass is needed in order to fire the thruster along the right direction.

Mass properties are often estimated performing calibration maneuvers, during which the large angular rates and accelerations of the slewing spacecraft can me measured and used to set up several Kalman filters that provide updated estimates of the inertia tensor, the location of the center of mass, and the total system mass.[6,7] These filters combine measurements from on-board instruments with first principles, such as conservation of angular momentum.[8] However, such maneuvers need specific calibration procedures involving large slews that can interrupt the spacecraft's nominal operations.[9] Moreover, large slews can excite the vibrational modes of flexible appendages such as solar arrays which can further complicate the estimation solution. Finally, rotating calibration maneuvers can move the fuel to different tank locations when when the ion thruster is causing the fuel to settle in the thrust direction of the tank. Other methods to estimate inertia properties involve the articulation of moving appendages: accurate knowledge of the mass and position of the appendage with respect to the body, combined with velocity measurements, allows to estimate the inertia properties for the whole system.[10]

This paper develops a technique to estimate the location of the CM of the system while thrust is continuously being applied, and the spacecraft's pointing requirements are being satisfied at all times. The motion platform supporting the thruster is gimbaled periodically to align the thrust vector based on the current CM estimate. Of interest is how these small platform orientation changes can be used to make the three-dimensional CM location observable. In this work, the steady-state response of the attitude control system with integral feedback constitutes the measurement model to inform the estimator on the torque produced by the offset between CM and thrust vector. The steady-state integral feedback term will account for the net external torque acting on the spacecraft system. The CM location is updated assuming this term is dominated by the CM uncertainty, but

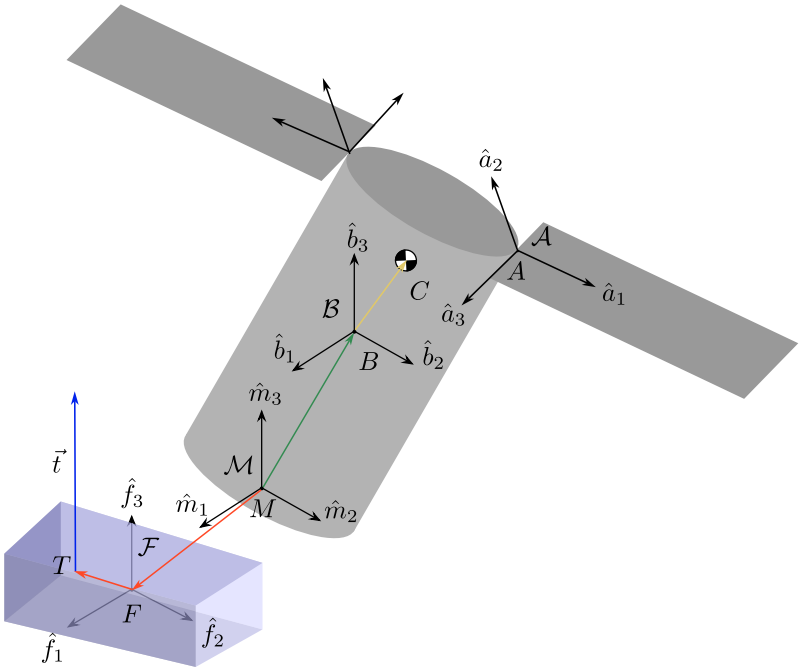

Figure 2: Spacecraft and gimbaled thruster sketch

will also consider the torques due to other external influences like solar radiation pressure. The study explores the effectiveness of this approach in an integrated mission scenario that enforces the inertial thruster pointing constraint and corrects the body and platform orientations to seek long-term thrusting without reaction wheel momentum build-up.

This paper begins by describing the low-thrust mission details and dynamic model. Subsequently, the paper explores how to perform continuous CM estimation leveraging the steady-state integral feedback term that compensates for external torques, leveraging aspects of the mission design choices. The estimation algorithm is outlined, and its limits are discussed. After outlining the simulation framework and the physical mass properties of the simulated components of the spacecraft, numerical simulations are presented to show the performance during short-term and long-term simulations.

SPACECRAFT MODEL

Hub

The spacecraft analyzed in this paper features several components. The main component is the spacecraft hub, whose motion affects the dynamics of all the connected components and is directly controlled by a system of reaction wheels. The body-frame $\mathcal{B}$ with origin in point B is fixed with respect to the hub, and it is the frame with respect to which measurements about the spacecraft attitude $\boldsymbol{\sigma}_{\mathcal{B}/\mathcal{N}}$, angular rates $\boldsymbol{\omega}_{\mathcal{B}/\mathcal{N}}$, and angular accelerations $\dot{\boldsymbol{\omega}}_{\mathcal{B}/\mathcal{N}}$ are provided. The law implemented to control the attitude of the hub is a nonlinear PID-like controller:[11]

$$\begin{aligned}\boldsymbol{u} = &-K\boldsymbol{\sigma}_{\mathcal{B}/\mathcal{R}} - P\boldsymbol{\omega}_{\mathcal{B}/\mathcal{R}} - PK_I\boldsymbol{z} + \\ &+ \boldsymbol{\omega}_{\mathcal{B}/\mathcal{N}} \times \left([\boldsymbol{I}_{\text{tot},C}]\boldsymbol{\omega}_{\mathcal{B}/\mathcal{N}} + [\boldsymbol{G}_s]\boldsymbol{h}_s\right) + [\boldsymbol{I}_{\text{tot},C}]\left(\dot{\boldsymbol{\omega}}_{\mathcal{R}/\mathcal{N}} - \boldsymbol{\omega}_{\mathcal{B}/\mathcal{N}} \times \boldsymbol{\omega}_{\mathcal{R}/\mathcal{N}}\right) \quad (1)\end{aligned}$$

where the first three terms constitute, respectively, the proportional, derivative, and integral terms, and $\boldsymbol{z} = K\int_{t_0}^{t}\boldsymbol{\sigma}_{\mathcal{B}/\mathcal{R}}\mathrm{d}t + [\boldsymbol{I}_{\mathrm{tot},C}]\boldsymbol{\omega}_{\mathcal{B}/\mathcal{R}}$. The other terms arise due to the gyroscopic couplings in Euler's equation of motion, and are needed in the nonlinear control law to ensure asymptotic stability. The tensor $[\boldsymbol{I}_{\mathrm{tot},C}]$ represents the inertia of the full system, minus the inertias of the reaction wheels about their respective spin axes. See Reference 11 for a detailed derivation of this control law. It is important to note that the tensor $[\boldsymbol{I}_{\mathrm{tot},C}]$ is, in general, not constant, because it factors in the inertias of moving components uncertainties on the inertias of the individual components, combined with uncertainties on the relative position between them, can make this tensor difficult to estimate. Such control law is designed to zero the relative attitude ($\boldsymbol{\sigma}_{\mathcal{B}/\mathcal{R}}$) and angular velocity ($\boldsymbol{\omega}_{\mathcal{B}/\mathcal{R}}$) between the body frame $\mathcal{B}$ and a reference frame $\mathcal{R}$. The integral term $PK_I\boldsymbol{z}$ has the ability to zero the bias in the steady-state response due to a constant, unmodeled torque acting on the system. As will be further discussed later, the integral feedback term fits well with the purpose of this work, where the assumption is that the unmodeled torques acting on the system are dominated by the thruster offset with the system's CM. Over an observation time window, the thruster application point does not change, nor does the thrust force, therefore the assumption of a constant unmodeled torque is valid.

Reaction Wheels

The spacecraft is actuated by means of four reaction wheels in a pyramid configuration as shown in Figure 3. The RW setup is such that two reaction wheels can provide torque about the first principal body axis ${}^{\mathcal{B}}\hat{\boldsymbol{b}}_1 = (1,0,0)^T$, two about the second principal body axis ${}^{\mathcal{B}}\hat{\boldsymbol{b}}_2 = (0,1,0)^T$, and all four contribute to the torques about the third principal body axis ${}^{\mathcal{B}}\hat{\boldsymbol{b}}_3 = (0,0,1)^T$, where the left superscript $\mathcal{B}$ is used to denote that the vector are expressed in the $\mathcal{B}$ frame. This is achieved by a 40 degrees upwards tilt angle in the direction of the wheels' spin axes $\hat{\boldsymbol{u}}_j$, and it is done to ensure that control about each axis is achievable even in the case of a single wheel failure. Given the

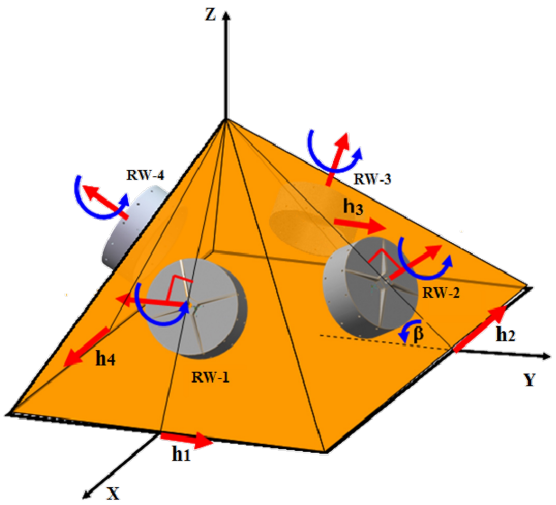

Figure 3: Four reaction wheels in pyramid configuration

following matrix $[\boldsymbol{G}_s] = [{}^{\mathcal{B}}\boldsymbol{u}_1, {}^{\mathcal{B}}\boldsymbol{u}_2, {}^{\mathcal{B}}\boldsymbol{u}_3, {}^{\mathcal{B}}\boldsymbol{u}_4]$ and under the assumption that the center of mass of each wheel is aligned with the respective spin axis, the rotational equations of motion of the wheels

are given by:

$$\boldsymbol{u}_{\text{RW}} = \dot{\boldsymbol{h}}_s = I_W(\dot{\boldsymbol{\Omega}} + [\boldsymbol{G}_s]^T \dot{\boldsymbol{\omega}}_{\mathcal{B}/\mathcal{N}}) \tag{2}$$

where $\boldsymbol{\Omega}$ contains the wheel speeds and I_W is the inertia of the wheels about the spin axis. The torques to the individual reaction wheels are computed by means of the minimum-norm solution, based on the requested torque in Equation (1):

$$\boldsymbol{u}_{\text{RW}} = -[\boldsymbol{G}_s]^T \left([\boldsymbol{G}_s][\boldsymbol{G}_s]^T\right)^{-1} \boldsymbol{u} \tag{3}$$

where $\boldsymbol{u}$ is the torque being exchanged between the RWs and the hub. Because the wheels are balanced and their respective axes do not change with respect to the hub, their motion does not affect the location of the CM of the system over time.

Solar Arrays

Each solar array is modeled as a rigid bodies attached to the hub by means of a single degree-of-freedom hinge. This hinge allows rotations about the spin axis $\hat{\boldsymbol{a}}_1$, which is required to enable the arrays to track the direction of incoming sunlight. The spin axis is fixed with respect to the body frame $\mathcal{B}$.

The motion of the system consisting of the hub and solar arrays is described by a system of three equations that relate to the translational motion of the CM of the system, three equations that relate to the rotation of the system, plus one equation for each solar array that describes the additional degree of freedom that allows the arrays to rotate about their hinge axis. The analytical derivation of the equations of motion is lengthy and out of the scope of this paper. For the details, the reader is referred to Reference 12. For the purpose of this analysis, the focus is given to the fact that the relative rotation between the hub and the arrays is controlled via a torque input. This is the torque exchanged between the hub and the array(s), and it has the form of a PD control law:

$$\boldsymbol{u}_{\text{SA}} = -\left[K_{\text{SA}}(\alpha - \alpha_R) + P_{\text{SA}}(\dot{\alpha} - \dot{\alpha}_R)\right] \hat{\boldsymbol{a}}_1 \tag{4}$$

where α is the relative angle between hub and arrays(s) and α_R is the reference angle that ensures maximum sunlight incidence on the array surface. In this work, the center of mass of the arrays is aligned with the spin axis, therefore the motion of the arrays does not affect the location of the CM of the system.

Thruster Platform

The platform and thruster assembly is modeled as a rigid body with negligible mass, attached to the lower surface of the spacecraft. The same considerations apply as for the solar arrays. In this case, two differential equations are required to describe the dynamics of the gimbal with respect to the hub, on top of the six equations that describe the translational motion of the CM and the rotation of the system. A two axis gimbal connects the platform to the main hub, allowing it to perform tip and tilt rotations with respect to the hub. As shown in Figure 2, the mount frame $\mathcal{M}$ is a frame fixed to the hub, whose origin M coincides with the contact point between the lower gimbal and the hub. Defining ν_1 and ν_2 the tip and tilt angles, respectively, the rotation of the platform frame $\mathcal{F}$ with respect to the body-fixed mount frame $\mathcal{M}$, is obtained as:

$$[\mathcal{FM}] = \begin{bmatrix} \cos\nu_2 & \sin\nu_1 \sin\nu_2 & -\cos\nu_1 \sin\nu_2 \\ 0 & \cos\nu_1 & \sin\nu_1 \\ \sin\nu_2 & -\sin\nu_1 \cos\nu_2 & \cos\nu_1 \cos\nu_2 \end{bmatrix} \tag{5}$$

where the tip angle ν_1 is about the $\hat{\boldsymbol{m}}_1$ axis and the tilt angle ν_2 is about the $\hat{\boldsymbol{f}}_2$ axis. The thruster-platform assembly is modeled analogously to the solar arrays, with the exception that there are, in this case, two degrees of freedom between the hub and the platform. The equations of motion are once again solved using the back-substitution method. The two gimbal angles are also controlled via torque inputs about the gimbal axes, once again according to PD control laws:

$$\boldsymbol{u}_{\text{PL}} = -\left[K_{\text{PL}}(\nu_1 - \nu_{R1}) + P_{\text{PL}}(\dot{\nu}_1 - \dot{\nu}_{R1})\right]\hat{\boldsymbol{m}}_1 - \left[K_{\text{PL}}(\nu_2 - \nu_{R2}) + P_{\text{PL}}(\dot{\nu}_2 - \dot{\nu}_{R2})\right]\hat{\boldsymbol{f}}_2. \quad (6)$$

It is important to notice that the thrust vector $\boldsymbol{t}$ is defined in platform frame coordinates, as it is applied to the platform. However, applying the back-substitution method, the force and torque resulting from the thruster's action are mapped into resulting force and torque on the whole assembly.

Equations of Motion at steady state

All the components described above interact with one-another via the exchange of forces and torques. To correctly describe the dynamics of the system in all its parts, 14 equations of motion are required. The equations of motion for the translation of the CM are not relevant to this problem. The rotational equations can be simplified considering the steady-state response of the solar arrays and thruster platform. In the assumption that there are no parasitic torques acting about the hinges and gimbals that connect these components to the hub, both Equations (4) and (6) are proven to drop to zero once the desired reference angles are tracked. The resulting rotational equations of motion are:

$$[\boldsymbol{I}_{\text{tot},C}]\dot{\boldsymbol{\omega}}_{\mathcal{B}/\mathcal{N}} = -\boldsymbol{\omega}_{\mathcal{B}/\mathcal{N}} \times ([\boldsymbol{I}_{\text{tot},C}]\boldsymbol{\omega}_{\mathcal{B}/\mathcal{N}} + [\boldsymbol{G}_s]\boldsymbol{h}_s) + \boldsymbol{L}_{\text{thr}} + \boldsymbol{L}_{\text{SRP}} + \boldsymbol{u} \quad (7)$$

where $\boldsymbol{u}$ is the control torque applied to the hub, as per Equation (1) and $[\boldsymbol{I}_{\text{tot},C}]$ is, again, the inertia of the entire system at steady state, minus the inertias of the RWs about their respective spin axes. Under the assumption that the solar arrays and the platform reach their respective steady-state response faster than the hub, it is valid to assume that $[\boldsymbol{I}_{\text{tot},C}]$ is constant in Equation (7), and that the system as a whole can be effectively treated as a whole rigid body. The control torques Equations (4) and (6) do not appear because, per hypothesis, at steady state their contribution is zero. Equation (2) provides the dynamics of the four reaction wheels. The term $\boldsymbol{L}_{\text{SRP}}$ is the solar radiation pressure torque acting on the system. In this work it plays the role of an unmodeled torque acting on the system, but in a real scenario there could be multiple such disturbances. The remaining torque, $\boldsymbol{L}_{\text{thr}}$, is the torque that the thruster is producing on the system, and it is better discussed in the following section.

It is interesting to take a closer look at the control law Equation (1) when the system converges on the desired reference frame $\mathcal{R}$. Because the reference is in first approximation static, in order to ensure inertial pointing of the thruster, it is $\boldsymbol{\omega}_{\mathcal{R}/\mathcal{N}} = \dot{\boldsymbol{\omega}}_{\mathcal{R}/\mathcal{N}} = 0$. Equation (1) is reduced to a regulator control law:

$$\boldsymbol{u} = -K\boldsymbol{\sigma}_{\mathcal{B}/\mathcal{N}} - P\boldsymbol{\omega}_{\mathcal{B}/\mathcal{N}} - PK_I\boldsymbol{z} \qquad \text{with} \qquad \boldsymbol{z} = K\int_{t_0}^{t}\boldsymbol{\sigma}_{\mathcal{B}/\mathcal{R}}\mathrm{d}t + [\boldsymbol{I}_{\text{tot},C}]\boldsymbol{\omega}_{\mathcal{B}/\mathcal{N}} \quad (8)$$

where the gyroscopic term $\boldsymbol{\omega}_{\mathcal{B}/\mathcal{N}} \times \left([\boldsymbol{I}_{\text{tot},C}]\boldsymbol{\omega}_{\mathcal{B}/\mathcal{N}} + [\boldsymbol{G}_s]\boldsymbol{h}_s\right)$ can be dropped without affecting the asymptotic stability properties of the control law,[11] and the inertial frame $\mathcal{R}$ is made coincide with the inertial frame $\mathcal{N}$, as it remains fixed in time. Additionally, once convergence to the reference frame is achieved, it is by definition $\boldsymbol{\sigma}_{\mathcal{B}/\mathcal{R}} \approx \boldsymbol{\omega}_{\mathcal{B}/\mathcal{R}} \approx 0$. When this steady-state condition is met,

the control torque is further reduced to:

$$\boldsymbol{u}_{\text{ss}} = -PK_I\boldsymbol{z} = -PK_IK\int_{t_0}^{t}\boldsymbol{\sigma}_{\mathcal{B}/\mathcal{R}}\mathrm{d}t \tag{9}$$

where effectively the control torque coincides with the integral feedback term, and any dependence on the inertia of the system is lost. This means that, once steady state is achieved, the control torque required to stabilize the system is not affected by potential errors in the inertia tensor, which in contrast would only affect the transient response.

CENTER OF MASS ESTIMATION

Traditional approaches

Traditional CM estimation algorithms, such as that outlined in Reference 7, rely on accelerometers mounted on the spacecraft hub. The measurement model is given by the relative acceleration theorem:

$$\boldsymbol{a} = \boldsymbol{a}_{CM} + \dot{\boldsymbol{\omega}}_{\mathcal{B}/\mathcal{N}} \times \boldsymbol{r} + \boldsymbol{\omega}_{\mathcal{B}/\mathcal{N}} \times (\boldsymbol{\omega}_{\mathcal{B}/\mathcal{N}} \times \boldsymbol{r}) + 2\boldsymbol{\omega}_{\mathcal{B}/\mathcal{N}} \times \dot{\boldsymbol{r}} \tag{10}$$

where $\boldsymbol{a}$ is the measured quantity, and $\boldsymbol{r}$ is the location of the center of mass to be estimated. Because the CM location is assumed to not vary over time ($\dot{\boldsymbol{r}} = 0$), and the system is not subject to external forces ($\boldsymbol{a}_{CM} = 0$), the equation above simplifies to the linear model:

$$\boldsymbol{a} = [\boldsymbol{H}(\boldsymbol{\omega}_{\mathcal{B}/\mathcal{N}}, \dot{\boldsymbol{\omega}}_{\mathcal{B}/\mathcal{N}})]\boldsymbol{r} \tag{11}$$

where the angular rates and accelerations of the hub are obtained from IMU measurements. These arguments, however, are not valid in the case of a thrust system such as the one considered in this paper. Because the external force acting on the system is not zero, the acceleration of the CM cannot be neglected:

$$\boldsymbol{a}_{CM} = \boldsymbol{t}/m \tag{12}$$

where $\boldsymbol{t}$ is the thrust vector, and m is the mass of the system, which are both subject to uncertainty. Moreover, because the thruster must be aligned with a certain inertial direction, the angular rates and accelerations of the hub are typically zero, except during transient control responses. This makes it such that the linear model in Equation (11) is very weakly dependent on the CM location $\boldsymbol{r}$, and therefore very weakly observable.

Measurement Model

This work is motivated by the need to perform continuous CM estimation over the extended periods of time during which the electric thruster is firing, without interrupting the nominal course of operations to perform calibration slew maneuvers to compute the exact location of the CM. The dynamics of the system when solar arrays and platform have reached steady-state response are given in Equation (7). With respect to Figure 2, the thruster torque on the system can be modeled as:

$$\boldsymbol{L}_{\text{thr}} = -\boldsymbol{r}_{C/T} \times \boldsymbol{t} = [\tilde{\boldsymbol{t}}]\boldsymbol{r}_{C/T} \tag{13}$$

where point T is the thrust application point, and it is known, and point C is the location of the CM, which is to be estimated.

Taking into consideration Equations (7), (12) and (13), and once again making the assumption that the system has converged to the reference frame, the following correlation can be highlighted between the integral feedback term and the thruster torque:

$$\boldsymbol{Z} = [\tilde{\boldsymbol{t}}]\boldsymbol{r}_{C/T} \tag{14}$$

where $\boldsymbol{Z} = PK_I\boldsymbol{z}$. Equation (14) constitutes a linear measurement model for the CM location, where the thrust direction vector $\boldsymbol{t}$ is, in first approximation, known, and the integral term $\boldsymbol{Z}$ is extracted from the flight software code segment that computes the torque delivered to the system by the reaction wheels at steady state. Because the platform orientation changes with time, so does the thrust application point T. For this reason, the measurement model can be better reformulated introducing point B, the origin of the body frame $\mathcal{B}$, whose coordinates are known and do not change over time. This allows to formulate the problem in terms of the position of the CM with respect to point B:

$$\boldsymbol{Z} + [\tilde{\boldsymbol{t}}]\boldsymbol{r}_{T/B} = [\tilde{\boldsymbol{t}}]\boldsymbol{r}_{C/B} \tag{15}$$

where $\boldsymbol{r}_{T/B}$ is the location of point T with respect to point B, and it can be measured very accurately thanks to the reliable knowledge of the angles of the stepper motor gimbal that controls the platform.

The main source of uncertainty is the thrust vector $\boldsymbol{t}$. While the mapping between the thruster-platform frame $\mathcal{F}$ and the body frame $\mathcal{B}$ is known accurately, the knowledge of the thrust vector in the ${}^{\mathcal{B}}\boldsymbol{t}$ frame is ultimately dependent on how accurately the thruster performance is known in its own frame ${}^{\mathcal{F}}\boldsymbol{t}$. This means that if the thruster is misaligned with the nominal direction, or if the magnitude of the thrust vector is off-nominal, this would affect the reliability of the measurement model. This work assumes, in first approximation, exact knowledge of the thrust vector ${}^{\mathcal{F}}\boldsymbol{t}$. Uncertainties in the model are discussed later.

Observability

Based on the considerations made in the previous subsection, it is possible to define the following system:

$$\begin{cases} \dot{\boldsymbol{x}} = [\boldsymbol{A}]\boldsymbol{x} \\ \boldsymbol{y} = [\boldsymbol{C}]\boldsymbol{x} \end{cases} \tag{16}$$

where $\boldsymbol{x} = \boldsymbol{r}_{C/B}$ is the quantity to be estimated and $\boldsymbol{y} = \boldsymbol{Z} - [\tilde{\boldsymbol{t}}]\boldsymbol{r}_{T/B}$ constitutes the measurement, and $[\boldsymbol{C}] = [\tilde{\boldsymbol{t}}]$ the linear model. With the assumptions made in this work, the CM location does not change over time, which means that $[\boldsymbol{A}] = 0_{3\times3}$. Analyzing the observability for a static configuration, i.e., a case in which the platform is not moving with respect to the hub, gives the following observability matrix:[13]

$$[\mathcal{O}] = \begin{bmatrix} \boldsymbol{C} \\ \boldsymbol{CA} \\ \vdots \\ \boldsymbol{CA}^{n-1} \end{bmatrix} = [\tilde{\boldsymbol{t}}]. \tag{17}$$

Because $[\tilde{\boldsymbol{t}}]$ is the skew-symmetric cross product matrix, it is known to have rank 2. This means that, in such static configuration, the CM location is not fully observable. This could be inferred thinking about the problem from a physical standpoint: when no torque is acting on the system, i.e., $\boldsymbol{Z} = 0$, it means that the thruster is being fired exactly through the system's CM. However, the exact position of the CM remains unknown, as it could lie anywhere along the thrust line.

However, as discussed in Reference 4, the thrust vector does not remain constant in body-frame coordinates, because the platform is actuated in order to perform momentum dumping. As a result, the measurement model is not static, but rather time-varying. In such case, the general observability matrix is expressed as:[14]

$$[\mathcal{O}] = \begin{bmatrix} \boldsymbol{C}(t) \\ \dfrac{\mathrm{d}}{\mathrm{d}t}\boldsymbol{C}(t) \\ \vdots \\ \dfrac{\mathrm{d}^{n-1}}{\mathrm{d}t^{n-1}}\boldsymbol{C}(t) \end{bmatrix}. \tag{18}$$

What this means in practical terms is that if the platform is held at a constant configuration, the problem is not fully observable. However, articulating the platform and taking measurements from different thruster-platform configurations, makes the problem fully observable even when the CM location has no dynamics.

Recursive Least-Squares Algorithm

The recursive LS algorithm implemented to estimate the location of the CM, effectively, coincides with the correction step of a Kalman filter. In other words, the algorithm is equivalent to a Kalman filter where the state has no dynamics, and therefore there is no prediction.

At every n-th measurement update, the following quantities are given:

- $\epsilon_n = \sqrt{|\boldsymbol{\sigma}_{\mathcal{B}/\mathcal{R}}|^2 - |\boldsymbol{\omega}_{\mathcal{B}/\mathcal{R}}|^2}$: convergence error
- $[\boldsymbol{C}_n] = [\tilde{\boldsymbol{t}}]$: linear model
- $\boldsymbol{y}_n = \boldsymbol{Z} + [\tilde{\boldsymbol{t}}]\boldsymbol{r}_{T/B}$
- $[\boldsymbol{K}_n]$: optimal gain
- $\boldsymbol{x}_n = \boldsymbol{r}_{C/B}$: CM location estimate
- $[\boldsymbol{P}_n]$: covariance of the state estimate.

The equations that define how to update each quantity at every step are, once again, those of the correction step in a regular Kalman filter:[13]

$$[\boldsymbol{K}_n] = [\boldsymbol{P}_n][\boldsymbol{C}_n]^T \left([\boldsymbol{C}_n][\boldsymbol{P}_n][\boldsymbol{C}_n]^T + [\boldsymbol{R}]\right)^{-1} \tag{19}$$

$$\boldsymbol{x}_{n+1} = \boldsymbol{x}_n + [\boldsymbol{K}_n]\left(\boldsymbol{y}_n - [\boldsymbol{C}_n]\boldsymbol{x}_n\right) \tag{20}$$

$$[\boldsymbol{P}_{n+1}] = \left([\boldsymbol{I}] - [\boldsymbol{K}_n][\boldsymbol{C}_n]\right)[\boldsymbol{P}_n]. \tag{21}$$

$[\boldsymbol{R}]$ is the measurement noise covariance, and is constant for every measurements. It is an estimate of how much the measurement is corrupted by unmodeled perturbance.

The convergence error ϵ_n is used as a measure of whether the system has reached the steady state. If ϵ_n it means that the system has not converged to the reference, therefore the integral term $\boldsymbol{Z}$ is not representative of the torque that the thrust is applying on the system. For this reason, measurements are only processed when the convergence error drops below a user-defined threshold $\epsilon_n < \bar{\epsilon}$, which is a tuning parameter for the algorithm and depends, among other things, on the gains of the attitude control law.

SIMULATION

Simulation Framework

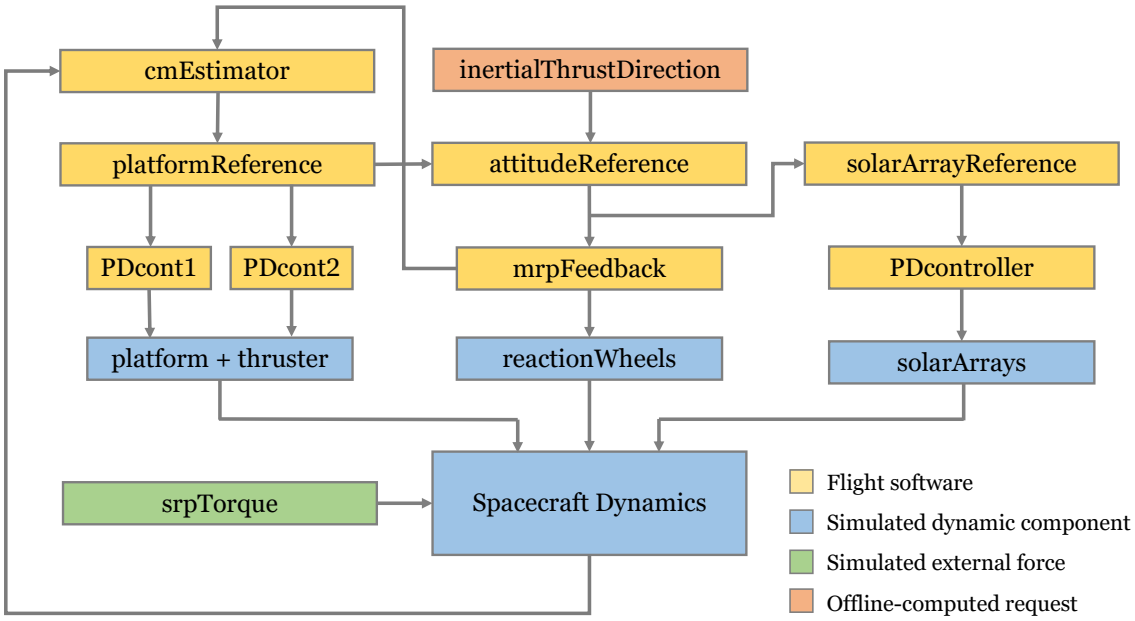

Figure 4: Simulation block diagram

The spacecraft is simulated using Basilisk Astrodynamics Simulation Framework*. Basilisk is an open-source software framework that can simulate complex spacecraft systems and behaviors. Its modular structure allows for building blocks, named modules, to simulate individual spacecraft components and/or flight software processes. Modules exist as standalone segments of code, with minimal interconnections. Exchanges of minimal information between modules limit the flow of information to what is strictly essential.[15,16]

Figure 4 illustrates the most relevant modules that are used in the simulations carried out in this paper. The reader is referred to References 4, 17 for a detailed description of what each code block represents within the simulation. This paper focuses on a fundamental difference between the block diagram in Figure 4 and the equivalent block diagram in Reference 4: in this previous contribution, the CM location is assumed to be known, the exact coordinates of the CM are pulled from the dynamic properties of the system, and fed into the `platformReference` module that computes the reference for the thruster platform. This is done for the purpose of testing the applicability of the control law that regulates the offset between the thrust vector and the CM for momentum dumping purposes. Realistically, however, this is a fundamentally wrong assumption, because a dynamic property such as the CM cannot just assumed to be known.

The main contribution of this paper consists in the development of the `cmEstimator` module. This new module extracts information from attitude measurements and flight software parameters,

*`https://hanspeterschaub.info/basilisk`

and uses them as a measurement model to inform a leas-squares (LS) algorithm that sequentially updates an initial guess of the CM location. The constantly-updated CM location estimate is fed to the `platformReference` module, which is in charge of articulating the thruster platform based on a best estimate of the CM location. For reasons that are better explained in the following sections, in this work the `platformReference` module is run at a slower frequency of $2.8 \cdot 10^{-4}$ Hz (one update every hour), compared to every other flight software component, which are run at 1 Hz (one update every second). The dynamics and the environment are run at a frequency of 10 Hz.

Spacecraft mass properties

The spacecraft hub is modeled as a cube with a 1.5 m side, a mass $m_{\text{hub}} = 750$ kg and the following inertia tensor, expressed with respect to a principal frame $\mathcal{B}$:

$$^{\mathcal{B}}[\boldsymbol{I}_{\text{hub}}] = \begin{bmatrix} 1531.4 & -5.1 & 7.9 \\ -5.1 & 2610.4 & 79.0 \\ 7.9 & 79.0 & 1998.4 \end{bmatrix} \text{ kg m}^2. \tag{22}$$

The solar arrays are modeled as thin discs with a diameter of 7 m, whose center of mass is located at 3.75 m from the hinges, along the rotation axis. The mass of the solar arrays is $m_{\text{sa}} = 5$ kg and the inertia tensor is:

$$^{\mathcal{A}}[\boldsymbol{I}_{\text{sa}}] = \begin{bmatrix} 17.5 & 0 & 0 \\ 0 & 35 & 0 \\ 0 & 0 & 17.5 \end{bmatrix} \text{ kg m}^2 \tag{23}$$

with respect to a principal frame $\mathcal{S}$.

The thruster is assumed to fire continuously, with a specific impulse $I_{\text{sp}} = 1600$ s and a thrust output of $t = 0.27$ N. In nominal conditions, the thrust is along the platform axis $^{\mathcal{F}}\hat{\boldsymbol{f}}_z = (0, 0, 1)^T$.

Mass depletion is not simulated in this work: that means that, even though the thruster is fired for extended periods of time, the mass of the system does not change. As a consequence, the location of the CM remains constant throughout the simulation. This is obviously a simplifying assumption. However, because the shift in the CM is primarily due to mass depletion, and because mass flow rate of electric thrusters is typically small, it is reasonable to assume that significant CM shifts happen over time scales that are much bigger than the time window in which the CM needs to be estimated.

NUMERICAL RESULTS

This section presents the results of the CM estimation algorithm applied to the simulation described in Figure 4. Based on the mass and inertia properties described in the Spacecraft Modeling section, the exact location of the CM with respect to origin B of the body frame is

$$^{\mathcal{B}}\boldsymbol{r}_{C/B} = (0.0961538, 0.0961538, -0.0108974)^T. \tag{24}$$

This is the quantity that needs to be estimated, and it is not known by the flight software a priori. The estimator module needs to be seeded with an initial estimate of the CM location, which plays a significant role in guaranteeing the success of the estimation and the stability of the simulation. The following results are obtained with initial estimate and covariance:

$$\boldsymbol{x}_0 = (0.06, 0.13, -0.05)^T \qquad [\boldsymbol{P}_0] = \begin{bmatrix} 0.0025 & 0 & 0 \\ 0 & 0.0025 & 0 \\ 0 & 0 & 0.0025 \end{bmatrix}. \tag{25}$$

Short-term simulation, no SRP

Figure 5 shows the results of the CM estimator over a simulation time of 3 hours. Subfigure (a) contains the errors on the three components of the CM location, computed as the difference between the current best estimate and the truth in Equation (24), together with the respective $\pm 3\sigma$ bounds. Additionally, each plot shows the convergence error ϵ. It can be observed that the first state update comes at around 30 seconds, when the convergence error drops below the threshold $\epsilon < \bar{\epsilon} = 10^{-6}$ and measurements start being processed. It is interesting to observe that two measurements are enough to bring the error on all three components of the state to a near-zero value. This is because while the problem is not fully observable with a single measurement, two linearly independent measurement are sufficient to resolve the three-dimensional estimation problem. For every 60-minute interval, it is possible to observe a sharp drop in the covariance and a change in the estimation error when the convergence threshold is met, while for the remainder of the 60-minute window these quantities appear to remain constant. In reality, they do vary during the remainder of the time window, due to the fact that the convergence of the attitude is asymptotic, and therefore the integral feedback term keeps evolving slightly. Looking at Figure 5 (b), it can be observed that the post-fit residuals do not have the typical white noise look, because the measurement noise is not, itself, randomly distributed.

More interesting information about the general behavior of the system can be inferred looking at Figure 6. Subfigures (a) and (b) show the tracking performance of the attitude and platform control systems as new references are generated for the platform every hour. Because the thruster's orientation with respect to the hub is updated every hour, the entire spacecraft has to rotate to

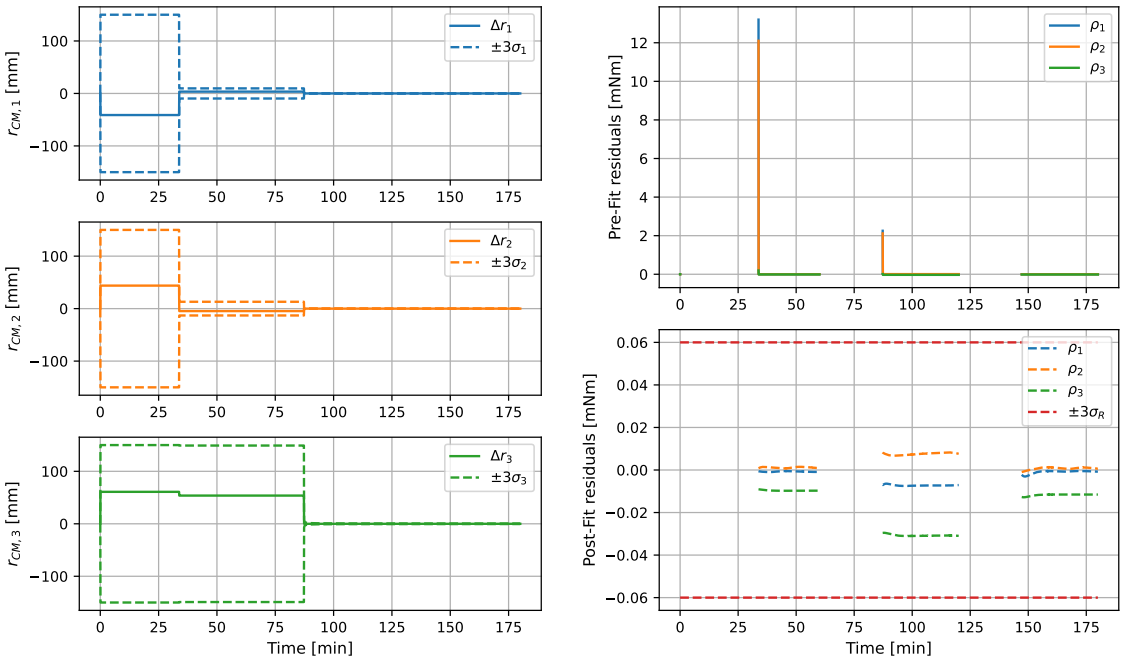

(a) State errors and covariances

(b) Residuals

Figure 5: CM estimation results

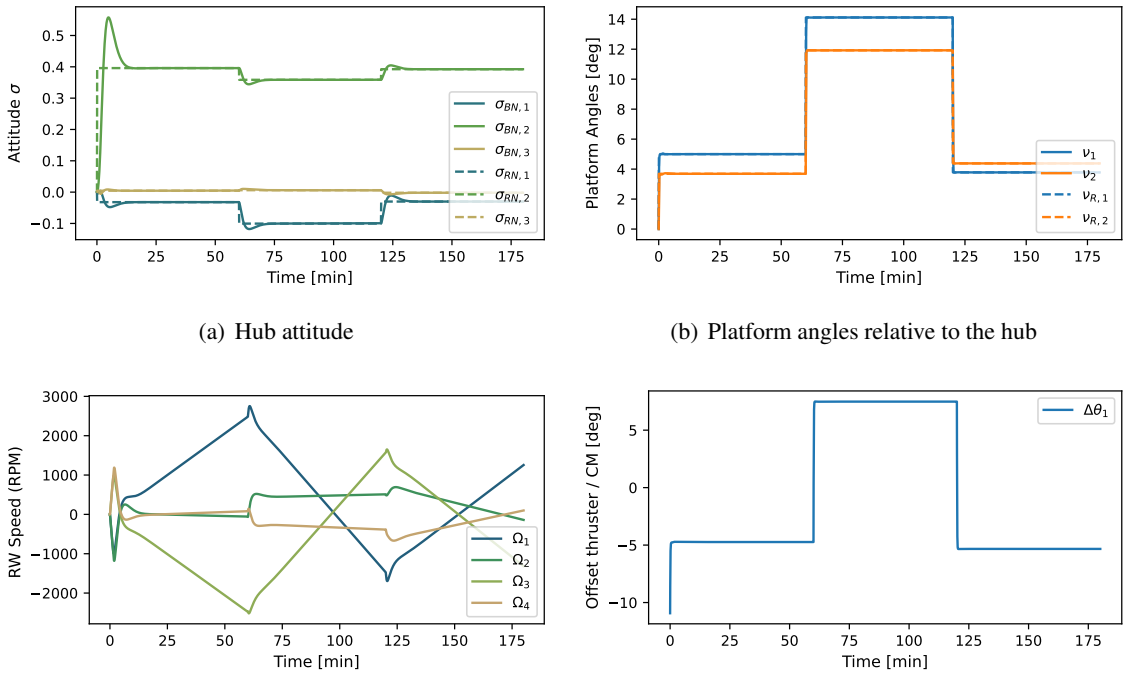

(a) Hub attitude

(b) Platform angles relative to the hub

(c) Reaction wheel speeds

(d) Thruster / CM angular offset

Figure 6: Spacecraft attitude and platform performance over time

accommodate the need to point the thruster inertially. The attitude plots show some transients that are larger for the initial reorientation maneuver, and become smaller and smaller subsequently when the only attitude change is due to the platform reorientation. Subfigures (c) and (d) give an insight on the momentum being accumulated on the reaction wheels. According to the control law outlined in Reference 4, the platform reference angles are computed based on the combination of most up-to-date knowledge of the CM location, and the total net momentum accumulated on the RWs. The control law will, therefore, offset the platform in order to use the thruster to dump the momentum on the wheels.

Long-term simulation, with SRP

It is interesting to observe what these results look like when the simulation is run for an extended period of time. Figures 7 and 8 show the same results over a time window of 3 days With SRP acting on the system. Figure 7 shows that even though the post-fit residuals are small, there is a bias on the estimated components of the CM location. This happens despite adding adding measurement noise covariance that is coherent with the magnitude of the SRP torque. Furthermore, it can be observed that none of the three components of the state settle on a constant value, but are rather affected by a long-term drift. The plots in Figure 8, however, show that despite the bias in the estimate. Similarly, the platform angles settle and the reaction wheel speeds do not saturate. Over the long-term simulation it is possible to observe that, coherently with the results shown in Reference 4, the RW speeds evolve in order to build momentum about the steady-state thrust vector direction, which is the direction about which momentum cannot be dumped.

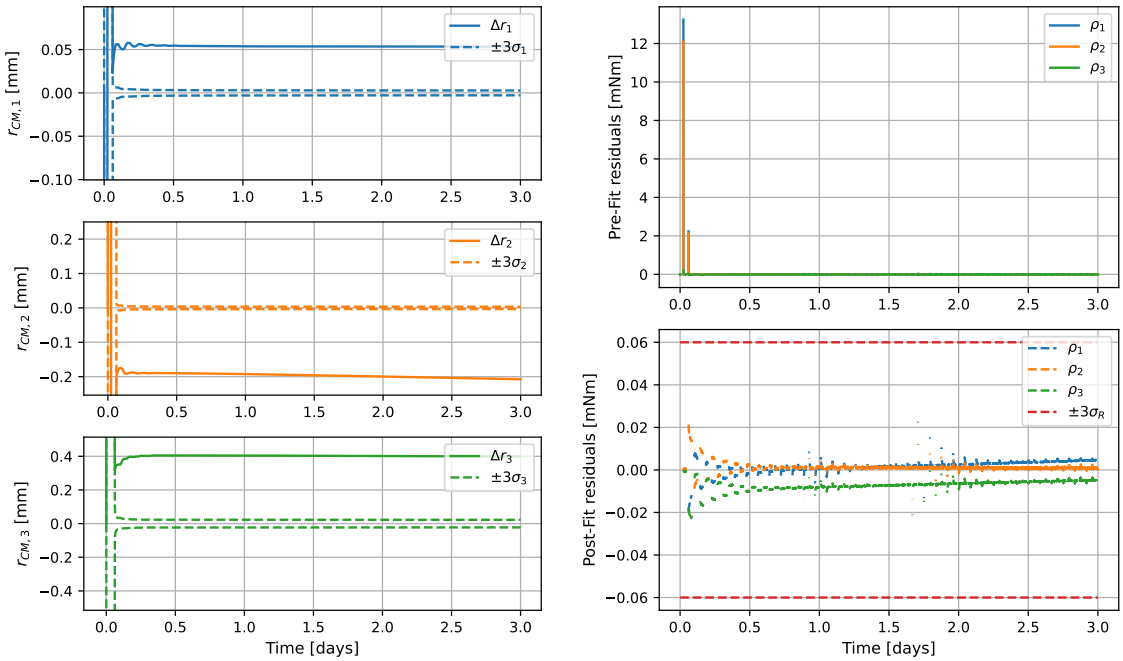

(a) State errors and covariances

(b) Residuals

Figure 7: CM estimation results

The steady-state bias can be explained by factoring the SRP torque into the model, and introducing point C^*:

$$\begin{aligned} \boldsymbol{Z} &= [\tilde{\boldsymbol{t}}]\boldsymbol{r}_{C/T} + \boldsymbol{L}_{\text{SRP}} \\ \boldsymbol{Z} &= [\tilde{\boldsymbol{t}}]\left(\boldsymbol{r}_{C/C^*} + \boldsymbol{r}_{C^*/B} + \boldsymbol{r}_{B/T}\right) + \boldsymbol{L}_{\text{SRP}} \\ \boldsymbol{Z} + [\tilde{\boldsymbol{t}}]\left(\boldsymbol{r}_{T/B} + \boldsymbol{r}_{C^*/C}\right) - \boldsymbol{L}_{\text{SRP}} &= [\tilde{\boldsymbol{t}}]\boldsymbol{r}_{C^*/B} \end{aligned} \tag{26}$$

where, at steady state, the measurement is affected by a constant bias. Due to the nature of the control law that actuates the platform, at steady state the thruster constantly dumps the momentum on the wheels. Consequently, in the presence of SRP, the thruster is not aligned with the center of mass, but instead with point C^*, such that the thruster torque is opposite to the SRP torque, minus the component along the thrust direction:

$$-\boldsymbol{r}_{C^*/C} \times \boldsymbol{t} = \boldsymbol{L}_{SRP} - \left(\boldsymbol{L}_{SRP} \cdot \hat{\boldsymbol{t}}\right)\hat{\boldsymbol{t}}. \tag{27}$$

Combining Equations (26) and (27) gives:

$$\underbrace{\boldsymbol{Z} + [\tilde{\boldsymbol{t}}]\boldsymbol{r}_{T/B} - \left(\boldsymbol{L}_{SRP} \cdot \hat{\boldsymbol{t}}\right)\hat{\boldsymbol{t}}}_{\boldsymbol{y}} = [\tilde{\boldsymbol{t}}]\underbrace{\boldsymbol{r}_{C^*/B}}_{\boldsymbol{x}} \tag{28}$$

which constitutes the effective measurement model in the presence of SRP torque. In the absence of SRP, Equation (28) coincides with Equation (15), and the result of the estimation is the actual CM location. Conversely, when SRP is acting on the system, the result of the estimation is the

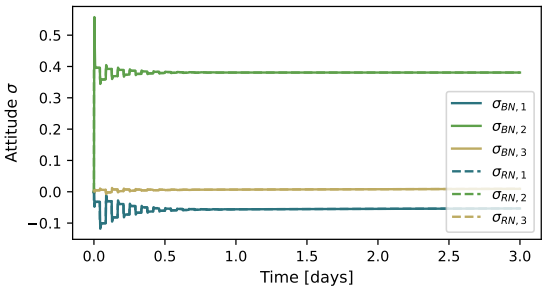

(a) Hub attitude

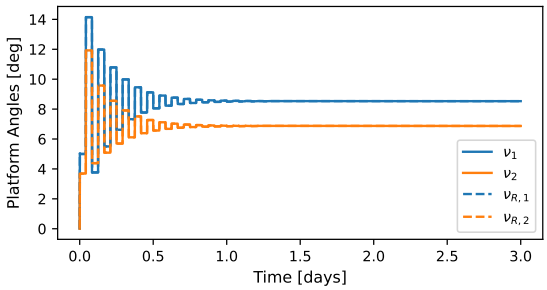

(b) Platform angles relative to the hub

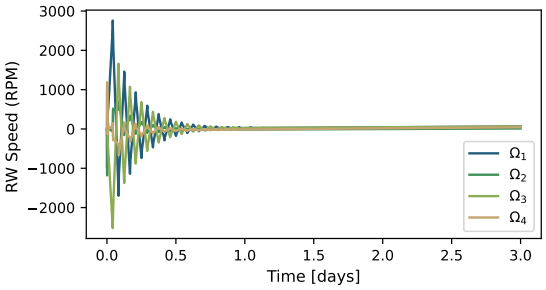

(c) Reaction wheel speeds

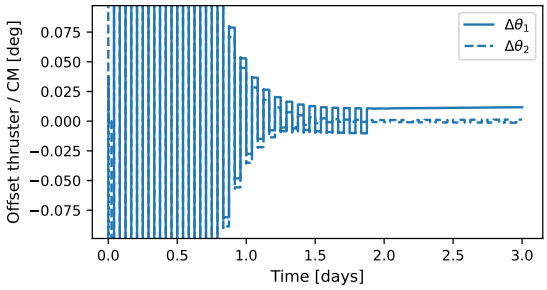

(d) Thruster / CM angular offset

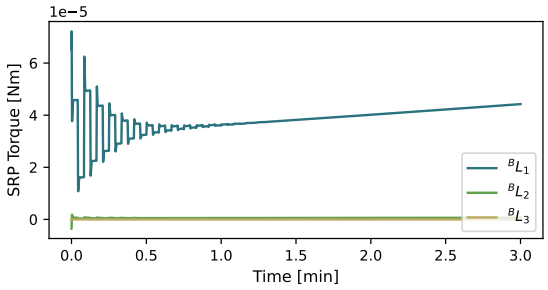

(e) SRP torque

Figure 8: Spacecraft attitude and platform performance over time

location of point C^*. When firing the thruster through point C^*, two out of three component of the SRP torque are neutralized, thus ensuring that momentum is constantly being dumped by the system. Figure 8 (d) shows, in fact, the different offsets between the thrust and the real center of mass ($\Delta\theta_1$), which shows a steady-state bias, and between the thrust vector and point C^* ($\Delta\theta_2$), which converges to zero at steady state.

CONCLUSIONS

This paper outlines a very simple algorithm to estimate the location of the center of mass of a spacecraft. This algorithm works in the presence of a gimbaled thruster that is consistently delivering a force and torque to the spacecraft system. This algorithm aims to close the loop on the problem of orienting the thrust vector in body-frame coordinates, for which knowledge of the CM location is required. This paper shows how the gimbaled thruster, which is the primary reason for CM estimation, can also be leveraged to deliver a solution to the CM estimation problem. Shortcomings of the algorithm are the many inaccuracies of the measurement model, where external forces can significantly corrupt torque measurements. Numerical simulations have shown that the CM can indeed be estimated accurately in the absence of unmodeled external disturbances. Specifically, the non-observable nature of the static problem is overcome by the articulating thruster, as the ability to thrust in different direction provides a set of linearly independent measurements that make the problem observable. Interesting results appear when external disturbances such as SRP are added to the system. While adding coherent measurement noise does not provide a good fix for such a biased measurement error, the combined action of the estimation algorithm with the platform control law is shown to drive the system to a stable configuration where momentum is being dumped continuously. The results suggest that, in the presence of a constant, unmodeled torque, the algorithm estimates not the location of the CM, but rather the location of a point through which the thruster torque cancels the unmodeled torque. This result is interesting and valuable because, despite not yielding the correct CM location, it drives the system to stability. This property can also be leveraged in the presence of a thruster misalignment, where incorrect knowledge of the thrust vector acts as an unmodeled disturbance and ultimately does not affect the ability to stabilize the system.

REFERENCES

[1] K. Holste, P. Dietz, S. Scharmann, K. Keil, T. Henning, D. Zschätzsch, M. Reitemeyer, B. Nauschütt, F. Kiefer, F. Kunze, *et al.*, "Ion thrusters for electric propulsion: Scientific issues developing a niche technology into a game changer," *Review of Scientific Instruments*, Vol. 91, No. 6, 2020, p. 061101, 10.1063/5.0010134.

[2] M. D. Rayman, T. C. Fraschetti, C. A. Raymond, and C. T. Russell, "Dawn: A mission in development for exploration of main belt asteroids Vesta and Ceres," *Acta Astronautica*, Vol. 58, No. 11, 2006, pp. 605–616, 10.1016/j.actaastro.2006.01.014.

[3] G. Racca, G. Whitcomb, and B. Foing, "The SMART-1 mission," *ESA bulletin*, Vol. 95, 1998, pp. 72–81, 10.1016/s0273-1177(99)00544-x.

[4] R. Calaon, L. Kiner, C. Allard, and H. Schaub, "Momentum Management Of A Spacecraft Equipped With A Dual-Gimballed Electric Thruster," *AAS Guidance and Control Conference*, Breckenridge, CO, Feb. 2–8 2023. Paper No. AAS-23-178.

[5] D. Y. Oh, S. Collins, D. Goebel, B. Hart, G. Lantoine, S. Snyder, G. Whiffen, L. Elkins-Tanton, P. Lord, Z. Pirkl, *et al.*, "Development of the Psyche mission for NASA's discovery program," *35th International Electric Propulsion Conference*, Atlanta, GA, October 8–12 2017.

[6] E. Bergmann, B. K. Walker, and D. R. Levy, "Mass property estimation for control of asymmetrical satellites," *Journal of Guidance, Control, and Dynamics*, Vol. 10, No. 5, 1987, pp. 483–491.

[7] E. Bergmann and J. Dzielski, "Spacecraft mass property identification with torque-generating control," *Journal of Guidance, Control, and Dynamics*, Vol. 13, No. 1, 1990, pp. 99–103.

[8] D.-H. Kim, D.-G. Choi, and H.-S. Oh, "Inertia estimation of spacecraft based on modified law of conservation of angular momentum," *Journal of Astronomy and Space Sciences*, Vol. 27, No. 4, 2010, pp. 353–357.

[9] S. Tanygin and T. Williams, "Mass property estimation using coasting maneuvers," *Journal of Guidance, Control, and Dynamics*, Vol. 20, No. 4, 1997, pp. 625–632.

[10] O. Ma, H. Dang, and K. Pham, "On-orbit identification of inertia properties of spacecraft using a robotic arm," *Journal of guidance, control, and dynamics*, Vol. 31, No. 6, 2008, pp. 1761–1771.

[11] H. Schaub and J. L. Junkins, *Analytical Mechanics of Space Systems*. AIAA, 4 ed., 2018, 10.2514/4.105210.

[12] J. Vaz Carneiro, C. Allard, and H. Schaub, "Rotating Rigid Body Dynamics Architecture For Spacecraft Simulation Software Implementation," *AAS Guidance and Control Conference*, Breckenridge, CO, Feb. 2–8 2023. Paper No. AAS-23-112.

[13] D. Simon, *Optimal state estimation: Kalman, H infinity, and nonlinear approaches*. John Wiley & Sons, 2006.

[14] E. D. Sontag, *Mathematical control theory: deterministic finite dimensional systems*, Vol. 6. Springer Science & Business Media, 2013.

[15] P. W. Kenneally, S. Piggott, and H. Schaub, "Basilisk: a flexible, scalable and modular astrodynamics simulation framework," *Journal of Aerospace Information Systems*, Vol. 17, No. 9, 2020, pp. 496–507.

[16] S. Carnahan, S. Piggott, and H. Schaub, "A New Messaging System For Basilisk," *AAS Guidance and Control Conference*, Breckenridge, CO, Jan. 30 – Feb. 5 2020. AAS 20-134.

[17] M. Cols-Margenet, H. Schaub, and S. Piggott, "Modular attitude guidance: Generating rotational reference motions for distinct mission profiles," *Journal of Aerospace Information Systems*, Vol. 15, No. 6, 2018, pp. 335–352.